Chemical Physics Letters 854 (2024) 141559

Contents lists available at ScienceDirect

Chemical Physics Letters

journal homepage: www.elsevier.com/locate/cplett

Research paper

Concentration effect of zinc ions on amyloid fibrillation of hen egg-white lysozyme with thermal treatment revealed by Raman spectroscopy

Muhammad Zahid [a,1], Ning Chen [a,1], Dongxiao Liu [a], Jionghan Wang [a], Lin Chen [b], Xiaoguo Zhou [a,*], Shilin Liu [a]

[a] Hefei National Research Center for Physical Sciences at the Microscale, Department of Chemical Physics, University of Science and Technology of China, Hefei, Anhui 230026, China

[b] School of Physics and Materials Engineering, Hefei Normal University, Hefei, Anhui 230601, China

ARTICLE INFO

Keywords:
Raman spectroscopy
Protein aggregation
Amyloid fibrils
Zn^{2+} ion
Hen egg white lysozyme

ABSTRACT

Accumulation of Zn^{2+} ions in protein aggregates has been suggested to be a key factor in Alzheimer's disease etiology. However, the specific influence of Zn^{2+} ions on the formation of amyloid fibrils or amorphous aggregates is still much debated. Herein, we conducted a combined study of Raman spectroscopy, UV–vis absorption spectroscopy and ThT fluorescence assay on the concentration effects of Zn^{2+} ions on amyloid fibrillation of hen egg-white lysozyme with thermal treatment. The addition of Zn^{2+} ions showed a negligible effect on unfolding of the protein tertiary structures and nucleation pathways on amyloid fibrillation. In contrast, a distinct concentration-dependence was observed for the influence of Zn^{2+} ions on the transformation of lysozyme secondary structures. At low concentration, the metal ions do not affect the populations of major secondary structures in the final state after incubation, while they at high concentration exhibit a promotion effect on the transformation from α-helix to β-sheet-like structures. These findings provide insights into the multifaceted impact of Zn^{2+} ions on protein aggregation, shedding light on potential therapeutic strategies for neurodegenerative diseases.

1. Introduction

Protein misfolding or erroneous folding can cause protein aggregation [1], leading to a class of disorders known as "protein conformational diseases", such as Parkinson's syndrome and Alzheimer's disease [2–4]. During the formation of these aggregates, protein molecules typically self-assemble into oligomers with random coil structures, then further form protofibrils and mature fibrils along the so-called "on-pathway" or amorphous aggregates with disordered structures such as the gel-like phase, which is called "off-pathway" [5]. As the oligomers are more cytotoxic for cells than fibrils [6,7], it is crucial to find suitable inducers to accelerate transformation from oligomers to fibrils or suppress the oligomer formation, for reducing cytotoxicity and even for disease therapeutics [8].

As one of soluble globular proteins, hen egg-white lysozyme (HEWL), comprising approximately 46 % α-helix and 6 % β-sheets in native state, has 40 % homology of peptide chain amino acid sequence with human lysozyme. Owing to similar active sites to amyloid-β (Aβ) peptides, HEWL is widely used as a model protein for amyloid fibrillation studies [9,10]. Many environmental factors have shown promotion or inhibitory effects on the HEWL denaturation kinetics, e.g. temperature [11], *p*H [12], the addition of small chemicals, such as succinimide [13], and nanoparticles [14]. Besides, metal ions have attracted wide attentions during past decades [15–17], since they are essential for life as catalytic or structural cofactors in about one-third of enzyme functions [18,19]. Cu^{2+} [20], Mg^{2+} [21], and Ni^{2+} [22] ions were reported to play an inhibitor role in the HEWL amyloid fibril formation under thermal and acidic conditions, while Cd^{2+} [23] and Mn^{2+} [24] play an accelerator role during amyloid fibrillation kinetics, especially in the secondary structure transformation from *α*-helix to organized *β*-sheets. More importantly, a more significant promotion influence of these metal ions was affirmed on the assembly into amorphous aggregates. In addition, in the absence of acids, Al^{3+} exhibits double-edged effects in HEWL amyloid fibrillation [25], that it can accelerate conformational transformations from α-helices to organized β-sheets, in addition to postponing α-helix degradation. Moreover, metal ion concentration-

* Corresponding author.
E-mail address: xzhou@ustc.edu.cn (X. Zhou).
[1] These authors contributed equally to this work.

https://doi.org/10.1016/j.cplett.2024.141559
Received 9 June 2024; Received in revised form 17 July 2024; Accepted 20 August 2024
Available online 22 August 2024

dependent influence was also observed, that finer fibers were found to dominate at low concentrations, while proteins preferred to form amorphous aggregates at high concentrations [22]. All these evidences imply complex and variable influence for transition metal ions on protein denaturation processes. Therefore, revealing the metal ion-specific effects on the formation of protein amyloid fibrillation is generally valuable, providing clues for in-depth understanding the association between the metal ions and protein denaturation.

Zinc, a vital transition metal element for human body, is pivotal in various physiological processes, including enzymatic reactions, immune function, DNA synthesis, and wound healing [26]. In principle, Zn^{2+} ions can bind to the N-terminal or some residues' side groups, such as the imidazole in histidine residues by electrostatic interactions [26,27]. This binding to Aβ may interfere with other functional expressions of zinc, inducing neurodegeneration [17]. Accumulating evidences indicate that prolonged or excessive exposure to Zn^{2+} ions can potentially lead to the onset or exacerbation of neurological disorders [28,29]. In contrast, it has been reported that zinc supplementation can improve the AD symptoms [30]. The contradictory conclusions imply that the influence of Zn^{2+} ions is more complex than we previously thought. Actually, Zn^{2+} ions were reported to play a positive role to promote the aggregation of Aβ peptides [26,31], on the contrary, Ma and his coworker showed an inhibitory effect of Zn^{2+} in the HEWL amyloid fibril formation under thermal and acidic conditions [32]. Apparently, there is no unified conclusion of the influence of Zn^{2+} ions in protein amyloid fibrillation until now. This gives us a motivation to conduct a thorough study on the concentration-dependent influence of Zn^{2+} on the amyloid aggregation kinetics of HEWL at the molecular level.

It is well known that acids are very strong inducers for protein denaturation, while metal ions are comparatively much weaker. Hereby, we have performed a series experiments of HEWL amyloid fibrillation in the absence or presence of Zn^{2+} ion at various concentrations with thermal incubation at 65 °C, without the addition of acids. Raman, UV–Vis absorption and Thioflavin T (ThT) fluorescence emission spectra of protein aqueous solutions have been measured. By analyzing the characteristic spectral peaks, we have investigated changes in the secondary and tertiary structure of proteins in the presence of metal ions, confirming the concentration-dependent role of Zn^{2+} ions in the amyloid fibrillation kinetics of HEWL. These insights clarify the influences of Zn^{2+} ions on protein aggregation at the molecular level.

2. Experimental

2.1. Protein solutions

HEWL used in current experiments was purchased from Sangon Biotech (Shanghai) Co. Ltd. and used without further purification. Thioflavin T (ThT) was purchased from Sigma-Aldrich, while other chemicals in reagent grade or better were purchased from Sinopharm. The initial HEWL concentration was set to be 20 mg/ml, and three solutions were prepared: two were mixed with Zn^{2+} ions, whose concentrations were 14 mM or 40 mM (the molar ratio of metal ion to lysozyme was 1:10 or 1:30), while the other was absent for metal ions. Then, the whole solutions were dispensed into multiple 5-mL sealed glass bottles and incubated at 65 °C for more than 200 h without agitation. At each specific incubation time, aliquots of the incubated protein solution was taken out from one vial and centrifuged at 12,000 g for 20 min to exclude gelatinous phase. The residual supernatant was used for Raman spectroscopy, ThT fluorescence, and UV–visible spectroscopy analyses.

2.2. Raman spectroscopy

Spontaneous Raman spectroscopy was performed as described elsewhere [33–35]. A CW laser (Coherent, Verdi 5, 532 nm, 4 W) beam was employed as the excitation light on the protein solution in a 10 mm × 10 mm quartz cuvette at room temperature. Scattered light was collected into a triple monochromator (Acton Research, TriplePro). A liquid–nitrogen-cooled CCD detector (Princeton Instruments, Spec-10:100B) was applied to record the spectra in the wavenumber region of 450–1850 cm^{-1} with a resolution of ~ 1 cm^{-1}. Raman shift was calibrated using mercury standard line. In order to achieve better signal-to-noise ratios, the acquisition time for each measurement was 1 min, and 10 acquisitions were averaged. In addition, the Raman spectra of pure protein were reliably obtained by subtracting the spectrum of water measured in identical conditions. As shown in our recent study [36], the uncertainty of peak position is usually lower than 1.0 cm^{-1}, and the error bar of Raman scattering intensity is less than 5 %.

2.3. ThT fluorescence assay

At each incubation time, 0.5 ml of the supernatant after centrifugation was diluted with 4.5 ml of ThT dyes (the concentration of 12 mg/L). An excitation wavelength of 409 nm was selected, and the fluorescence emission spectra of the mixed solutions were recorded using a fiber optic spectrometer (AvaSpec-ULS2048, Avantes) in the wavelength of 400–800 nm. The excitation laser power was set as 20 mW to ensure no saturation effect, and the fluorescence intensity at 477 nm was plotted with the incubation time to indicate the population variation of cross β-sheet-rich structures in amyloid fibrillation. All measurements were performed under ambient conditions.

2.4. UV–Vis absorption spectroscopy

Using a commercial spectrophotometer (Shimadzu, UV-2550), UV–Vis absorption spectrum of the supernatant was recorded in the wavelength range of 220–500 nm. To avoid saturation absorption at high concentration, the supernatant was diluted 20 times before measurements. Dilutions and spectra measurements were done at room temperature. In addition, as only soluble proteins were detected in the supernatant, the current absorption spectroscopic analyses were different from turbidity assays commonly used in the field of protein pharmaceuticals, where protein solution including soluble and insoluble components was directly measured without centrifugation.

3. Results and discussion

3.1. Influence of Zn^{2+} ions on the formation kinetics of soluble aggregates

It is well known that under thermal induction, protein molecules will gradually aggregate into soluble oligomers, protofibrils, up to mature amyloid fibrils or amorphous aggregates. According to more significant cytotoxicity of the oligomers [7], it is of great important to reveal the effect of Zn^{2+} ions on the formation of soluble aggregates.

A dominant absorption band of the HEWL supernatants is centered at 280 nm with a red-side tail extending to ~ 400 nm. This tail is attributed to the absorption of the forming soluble aggregates, and the corresponding absorbance at 350 nm is an efficient indicator for the population of soluble aggregates (especially oligomers) [24]. In addition, considering that the protein concentration was significantly varied in amyloid fibrillation, the concentration-normalized absorption spectra of the supernatants after incubation in three experimental conditions was plotted in Fig. 1 by using the absorbance at 280 nm.

With the incubation time, the absorption intensity of the tail between 325 and 380 nm gradually increases, in line with the formation of soluble aggregates. In the final state, the absorbance at 350 nm is further enhanced with the addition of zinc ions, especially at high concentration (40 mM), where the absorbance is nearly doubled. This clearly indicates that Zn^{2+} ions can promote the formation of soluble aggregates, which agrees with previously reported effects as an accelerator [37,38]. However, UV–Vis absorption spectroscopy as a nonspecific method cannot provide detailed structure information of aggregates formed during thermal amyloid fibrillation of HEWL.

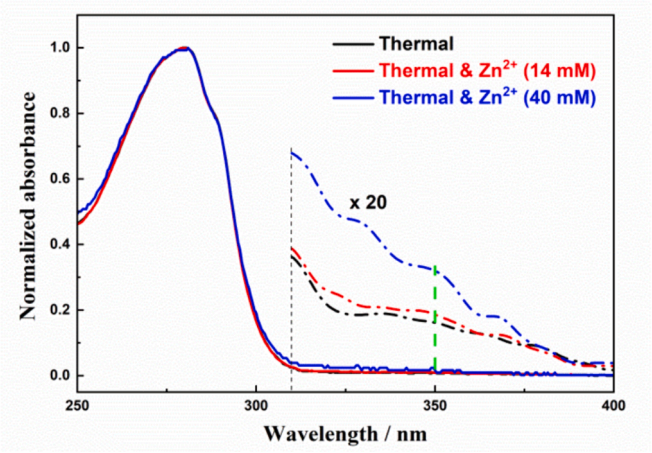

Fig. 1. UV–Vis absorption spectra of the HEWL supernatants after incubation at 65 °C for 200 h, where spectral intensity was normalized using the absorbance at 280 nm to eliminate the influence of protein concentration, and dash dotted lines represent the spectra amplified by a factor of 20.

3.2. Raman spectroscopy on changes of HEWL tertiary structure

As a powerful and sensitive approach for detecting secondary and tertiary structures of proteins in aqueous solutions, Raman spectroscopy has been widely used in the study of protein amyloid fibrillation [39–42]. Fig. 2 shows the Raman spectra of HEWL in the final state after incubation for 200 h in the range of 450–1850 cm^{-1}. Notably, when we compare the spectra of different incubation stages as shown in following sections, spectral intensities have been normalized with the absorbance at 280 nm to exclude the influence of protein concentration [12]. Six Raman spectral peaks have been commonly used to real-time monitor the structural changes of lysozyme [39,43,44], which are noted with color boxes in Fig. 2.

As the in-phase symmetric breathing vibration of phenyl ring of tryptophan (Trp) residues on HEWL side chains (at 759 cm^{-1}), together with the Trp Fermi resonance (so-called "W7" mode, located at 1340 and 1360 cm^{-1}), is sensitive to their micro-environments, especially hydrophobic interactions, the full width at half maximum (FWHM) of 759 cm^{-1} and the relative intensity ratio of I_{1340}/I_{1360}, are thought as two powerful indicators for protein tertiary structures [45–47]. As shown in the magnified spectra of Fig. 3a, the FWHM at 759 cm^{-1} is slightly broadened from 7.4–7.5 cm^{-1} to 8.4–8.7 cm^{-1}, in line with the more variegated conformations of Trp residues after incubation owing to unfolding of protein tertiary structures [48]. Likewise, the I_{1340}/I_{1360} ratio is increased from less than 1.0 to more than 1.0 (Fig. 3b), indicating that the local environment of Trp indole rings is exposed from a hydrophobic one to aqueous medium [45,49,50]. However, no visible difference is observed with these two indicators with the addition of Zn^{2+} ions, implying the metal ions have no significant effect on tertiary structures of protein in the final state.

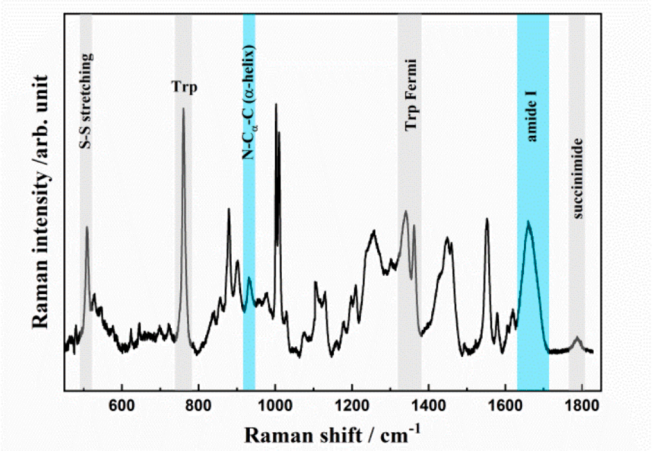

Fig. 2. Raman spectrum of the HEWL aqueous solutions in the final state after incubation for 200 h, where grey and cyan boxes are spectral indicators for tertiary and secondary structures.

Moreover, it is well known that the peak intensity of S-S stretching vibration at 507 cm^{-1} is proportional to populations of disulfide bonds, which is another common probe of tertiary structures [51–53]. As shown in Fig. 3c, the decrease in its intensity indicates partially disruption of disulfide bonds. Additionally, the peak intensity at ca. 1790 cm^{-1} has been proposed recently as the indicator for succinimide-like intermediates [36]. As the succinimide formation is associated with the deamidation of Asp residues [54,55], it is thought to play a crucial role in the nucleation process for protein amyloid fibril formation [56–58]. Notably, although it arises from the dehydration of the Asp-Gly dipeptide structures on protein backbone, its intensity change is sensitive to the variations of the local environment of Asp residues [36] as an efficient indicator for tertiary structures. In current experiments, this peak is observed indeed in all spectra of the final state under three conditions (Fig. 3d), in consistence with the formation of succinimide intermediates during amyloid fibrillation. According to these spectral evidences, an insignificant effect of Zn^{2+} ions is confirmed on the unfolding of lysozyme tertiary structures with thermal treatment at 65 °C. In other words, the action of Zn^{2+} ions has a much weaker influence than thermal effects.

3.3. Raman spectroscopy on transformation of HEWL secondary structure

For quantitative analysis of transformation of lysozyme secondary structures, two known indicators were used here: (1) the N-C_α-C stretching vibration of HEWL skeleton at 933 cm^{-1} is closely associated with α-helical structures, and its intensity is directly proportional to the content of α-helical structures [40,59]; (2) the amide I band covering the range of 1620–1700 cm^{-1} is attributed to the coupling mode of the C–O and C–N stretching vibrations and a small amount of N–H in-plane bending vibration of amide groups [40], and hence various protein secondary structures have different vibrational frequencies, e.g. the contribution of α-helix typically is located at 1650–1660 cm^{-1}, organized β-sheet structures is at 1670–1673 cm^{-1} [60], β-turns and random structures at 1670–1680 cm^{-1} [48], extended PP II structures in original fibers at 1667 cm^{-1} [44], intermolecular β-structures at 1669 cm^{-1} and random structures at 1680–1690 cm^{-1} respectively.

As shown in Fig. 4a, a moderate decrease (~26 %) in the spectral intensity at 933 cm^{-1} is observed after incubation, verifying partial loss of α-helical structures. It is worth noting that according to the previous study [50], the peak at 933 cm^{-1} almost disappears when the protein is completely transformed to amyloid-like fibers. Thus, only partial (~26 %) α-helical structures are transformed with the action of thermal and/or metal ions in our experiments. Notably, no significant difference is observed with the addition of Zn^{2+} ions. Furthermore, the blue shift of the peak position of the amide I band is usually to exhibit the transformation of α-helical structures to β-sheets or random structures [61]. As shown in Fig. 4b, the amide I peak position of the native state is located at 1658 cm^{-1}, in agreement with the fact that the predominant secondary structures of HEWL is α-helix. After incubation, the peak position remains almost unchanged, but the amide I band is slightly broadened, implying that other secondary structures are formed from the disrupted α-helix, although α-helical structures still occupies the major component of secondary structures.

As mentioned above, the amide I band includes all contributions of various secondary structures. Thus, the indicator of peak position does not provide all structure information of the transformation among these

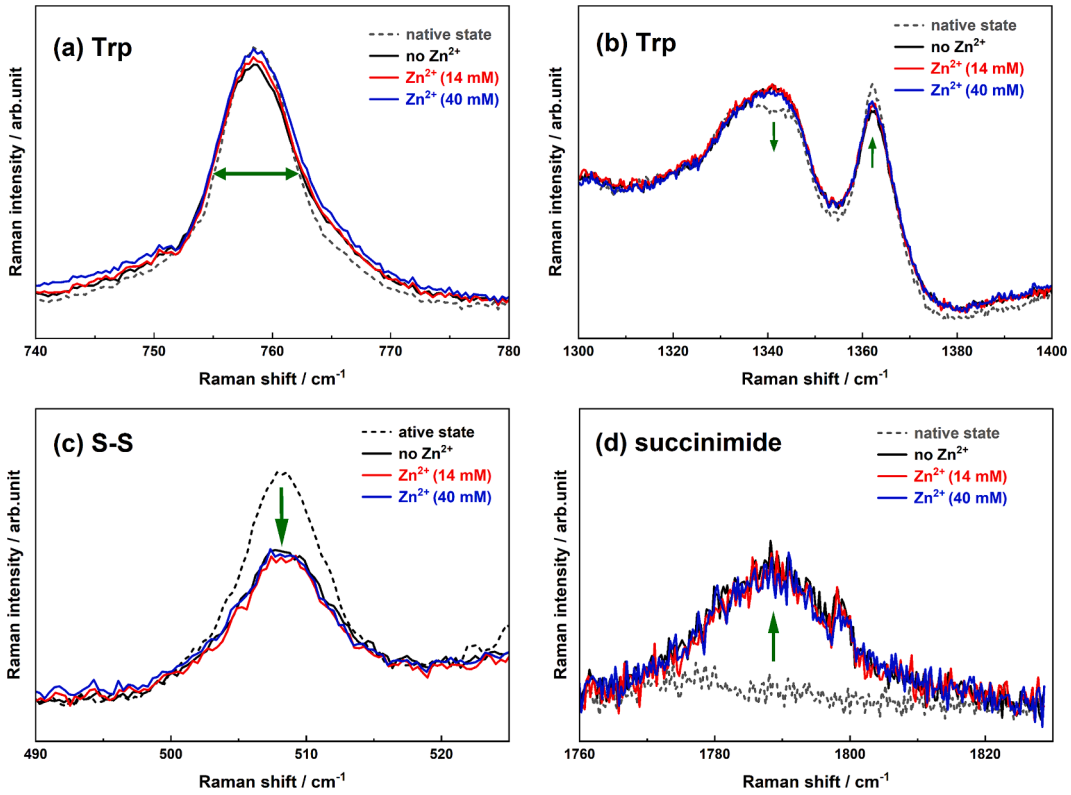

Fig. 3. Magnified Raman spectra of the HEWL supernatants in the ranges of (a) 740–780 cm^{-1}, (b) 1300–1400 cm^{-1}, (c) 490–520 cm^{-1}, (d) 1760–1830 cm^{-1}, after incubation at 65 °C for 200 h, where spectral intensity was normalized using the absorbance at 280 nm. The black, red, and blue curves are recorded in the absence and presence of Zn^{2+} ions with concentrations of 14 mM and 40 mM, respectively, while the dashed line is that of protein in native state for comparison.

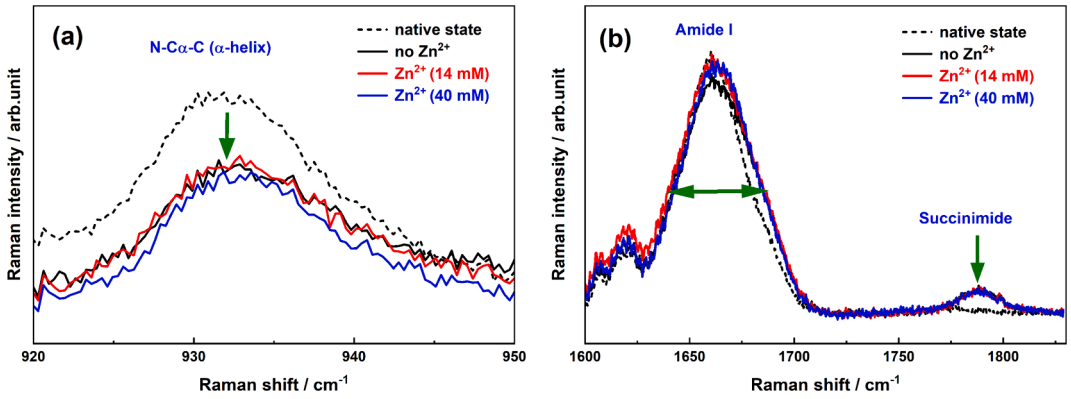

Fig. 4. Magnified Raman spectra of the HEWL supernatants in the ranges of (a) 920–950 cm^{-1} and (b) 1600–1830 cm^{-1}, after incubation at 65 °C for 200 h, where spectral intensity was normalized using the absorbance at 280 nm. The black, red, and blue curves are recorded in the absence and presence of Zn^{2+} ions with concentrations of 14 mM and 40 mM, respectively, while the dashed line is that of protein in native state for comparison.

conformers. To further exhibit the distribution change of different secondary structures, a multi-peak fitting was performed for this band profile as done previously [12,23]. Because the vibrational frequencies of amide I band of organized β-sheets, β-turns, intermolecular β-structures and extended PP II structures are very close, we used one peak with the center at 1669–1672 cm^{-1} to represent their joint contributions (named as the "β-sheet-like" structures), and the other three peaks were selected with the centers at ~ 1660 cm^{-1} for α-helical structures, 1645 cm^{-1} for random coils and 1686 cm^{-1} for random structures, respectively. Two additional peaks with the centers at 1606 and 1618 cm^{-1} were added to represent the contributions of the combined bands of the Tyr Y2 and the Phe F1 modes and the Y1 mode of Tyr residues, respectively [62,63].

Fig. 5 exhibits the fitting results for the amide I band of the HEWL supernatants, where the relative populations of dominant secondary structures are summarized in Table 1. In the native state, the secondary structures of HEWL consist predominantly of α-helix (51 %) and a certain amount of β-sheet-like structures (24 %), in general agreement with the result of X-ray crystal structure analyses of HEWL [64], where approximately 46 % α-helix were found.

The relative populations of these secondary structures are significantly changed after incubation, as indicated in Table 1. In the absence of metal ions, the secondary structures of the final state consist of random coils for 15 %, α-helix for 43 %, β-sheet-likes for 30 %, and random structures for 12 %. In comparison to the native state, the transformation from α-helix to β-sheet-like structures or random

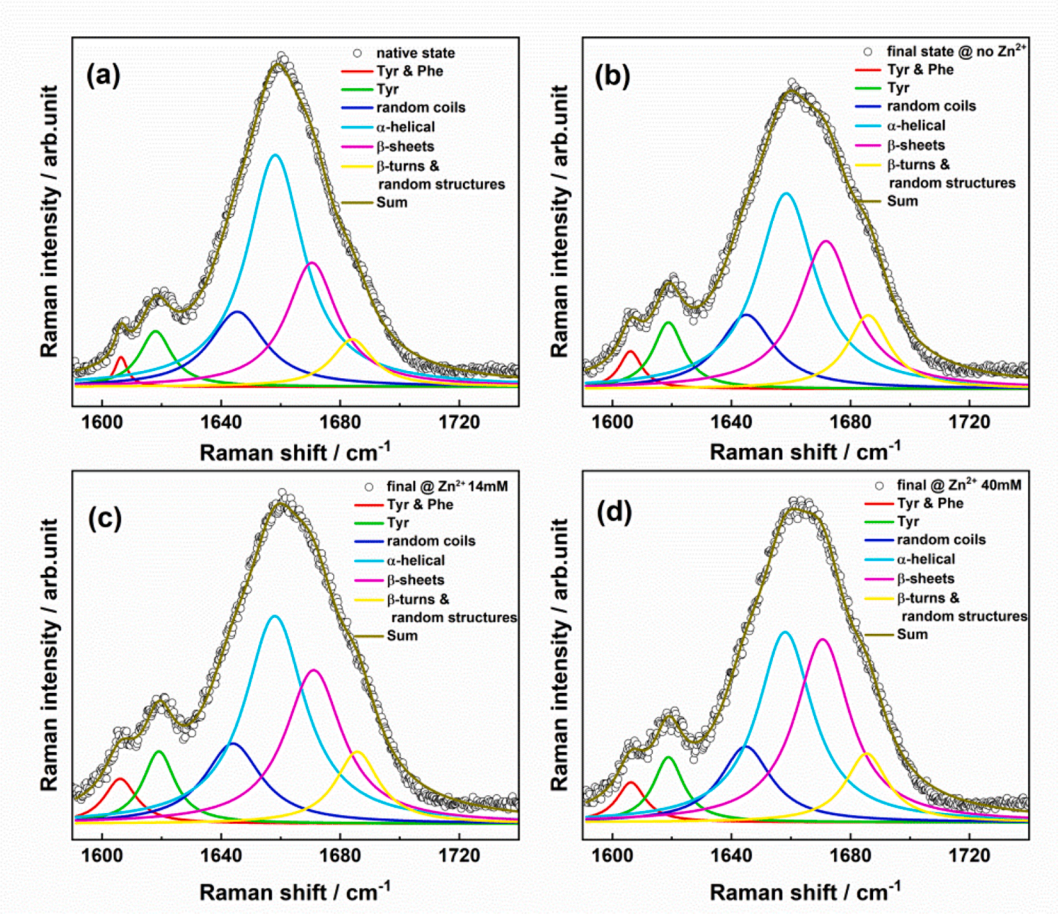

Fig. 5. Experimental and fitted amide I band of the HEWL supernatants in (a) the native state, and the final state with (b) thermal, (c) thermal/Zn^{2+} (14 mM), and (d) thermal/Zn^{2+} (40 mM) treatments, where six Lorentzian-type functions are used to present the contributions of major secondary structures and Tyr (and Phe) residues.

Table 1
Curve-fitting analysis of the amide I Raman band profile of the HEWL supernatants with thermal and thermal/Zn^{2+} treatments, where the unit of peak position is cm^{-1}, and the relative population of each component is shown as the peak area (%).

Incubation time /h	Random coils		α-helix		β-sheet-likes		Random structures	
	peak position	area	peak position	area	peak position	area	peak position	area
0	1645	17	1658	51	1671	24	1685	8
200 @ Zn^{2+} (0 mM)	1645	15	1658	43	1671	30	1686	12
200 @ Zn^{2+}(14 mM)	1644	16	1658	43	1671	30	1686	11
200 @ Zn^{2+}(40 mM)	1645	15	1658	38	1671	37	1685	10

structures is clearly observed. About 16 % of α-helix (the population is reduced from 51 % to 43 %) is disrupted, generally in line with the result (~26 %) of the N-C_α-C indicator at 933 cm^{-1}. Moreover, these relative populations are almost unchanged with the addition of Zn^{2+} ions at low concentration (14 mM), implying a weak effect of the metal ions. However, under high concentration, Zn^{2+} ions exhibit a considerable influence on distributions of various secondary structures. With the action of Zn^{2+} at the concentration of 40 mM, the populations of the secondary structures are determined by fitting to be 38 % for α-helix, 37 % for β-sheet-like structures, 15 % for random coils and 10 % for random structures. Obviously, the addition of the metal ions promotes the transformation of the α-helix to the β-sheet-like structures. To be fair, although the accuracy of the fitting is not satisfactory, it still provides solid evidence for the Zn^{2+} ions as an accelerator in amyloid fibrillation of HEWL with thermal treatment.

3.4. *ThT fluorescence assay*

ThT fluorescence is a widely used probe for detecting amyloid fibrils, and is thought to be a "gold standard" for cross β-sheet-rich structures [45,49]. Generally, the ThT molecule has low fluorescence quantum yield in aqueous solutions, but this fluorescence intensity is significantly enhanced when binding to highly ordered fibrillar aggregates. However, it is worth noting that this enhancement does not confirm the formation of mature fibrils, since an increase of ThT fluorescence intensity may be associated with the formation of non-fibrillar low-molecular-weight protein aggregates or non-crystalline assemblies [65]. Thus, we need to pay special attention to the magnitude of fluorescence enhancement in experiments.

Fig. 6 illustrates the ThT fluorescence spectra of the native-state lysozyme and the final products after incubation for 200 h, in the absence and presence of Zn^{2+} at two concentrations. Obviously, the peak shape is basically unchanged. For the aqueous solution of the native

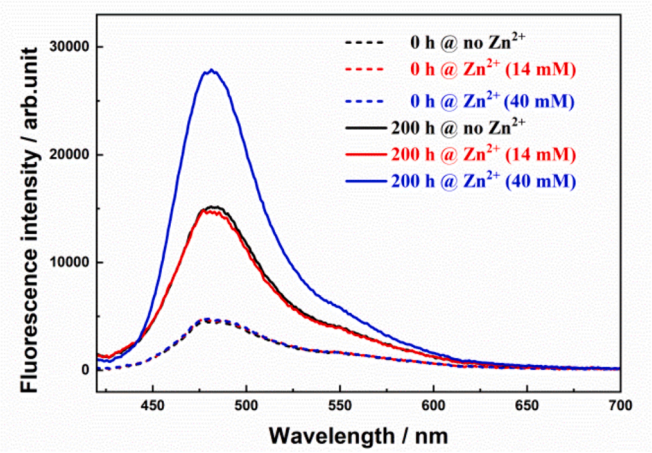

Fig. 6. ThT fluorescence spectra of the HEWL supernatants in (a) the native state, and the final state in (b) thermal, (c) thermal/Zn^{2+} (14 mM), and (d) thermal/Zn^{2+} (40 mM) conditions, with photoexcitation at 409 nm.

lysozyme, the fluorescence intensity is very weak due to the limited content of β-sheet structures. After incubation without metal ions, the fluorescence intensity increases by only 3-fold, indicating an elevated content of β-sheet structures with prolonged incubation time. Interestingly, when the Zn^{2+} ions with a low concentration (14 mM) were added into the solution, no additional enhancement of fluorescence intensity was observed. Thus, a negligible influence in the formation of β-sheet-rich structures is affirmed for Zn^{2+} ions at low concentration.

In contrast, in the presence of Zn^{2+} at the high concentration of 40 mM, the fluorescence intensity at the end time is enhanced by 6-fold, as shown in Fig. 6. This clearly confirms the promotion effect of Zn^{2+} on the formation of β-sheet structures, which agrees with the above conclusions of our Raman spectroscopy. Notably, this is opposite to the conclusion of Ma and his co-workers' Raman spectroscopy study [32], in which an inhibitor effect has been proposed for Zn^{2+} ions on amyloid fibrillation of HEWL. However, in Ma et al.'s experiment, protein solutions were adjusted to pH 2.0. We know, strong acidity is a very stressful condition for protein amyloid fibrillation kinetics. At pH 2.0, the disruption of all α-helix occurs within 40 h, and subsequently β-sheets are gradually formed in ~ 90 h [50]. With the action of acid, amyloid fibrils are dominantly produced along "on-pathway", while the "off-pathway" to gel-like aggregates is suppressed. In contrast to acid, Zn^{2+} ion is a relatively weak inducer. Considering that metal ions usually have strong electrostatic and coordination interactions with negatively charged amino acid residues on protein chain, these metal ions might have the potential to retard the breaking of protein secondary structure by acids. Actually, this postponement effect has been observed for Al^{3+} ions on amyloid fibrillation of HEWL indeed [25]. Generally, Zn^{2+} is considered to act on peptides or proteins through electrostatic interaction or coordination. It can bind with the N-terminal or some residues' side groups, like the imidazole in histidine residues. The coordination of the metal ions would reach saturation with the ion concentration increasing. Thus, it is generally probable that the metal ions perform a concentration-dependence, and maybe even a variety for proteins differing in morphology, associated with exposure of ligands.

4. Conclusions

In this work, a combined spectroscopic analysis of Raman, ThT fluorescence, and UV–vis absorption was performed to elucidate the influence of Zn^{2+} ions on amyloid fibrillation of HEWL with thermal treatment. As an indicator of soluble aggregates, the enhanced absorbance at 350 nm was found with the addition of zinc ions. Moreover, the greater the concentration, the more pronounced the enhancement. All these evidences confirm the promotion role of Zn^{2+} ions on protein aggregation.

Using three Raman indicators for protein tertiary structures, partial unfolding of the HEWL tertiary structures were observed after incubation for 200 h, but the addition of Zn^{2+} ions showed a negligible effect. Furthermore, the appearance of the peak at 1790 cm^{-1} under three conditions validates the formation of succinimide-like intermediates, indicating that Zn^{2+} ions do not change the nucleation pathways on the HEWL amyloid fibrillation. In contrast, a Zn^{2+} concentration-dependent influence was observed for the transformation of protein secondary structures. The relative populations of major secondary structures, such as α-helix, β-sheet-like structures, random coils, and random structures, remain unchanged in the final state after incubation for 200 h, when Zn^{2+} ions at low concentration (14 mM) are added into the solutions. However, at the high concentration of 40 mM, Zn^{2+} ions exhibit a promotion effect on the transformation from α-helix to β-sheet-like structures. This influence was further affirmed by ThT fluorescence assay. These insights provide more clues for the action mechanisms of Zn^{2+} ions on underlying protein aggregation at the molecular level and offer potential implications for therapeutic interventions in related neurodegenerative diseases.

CRediT authorship contribution statement

Muhammad Zahid: Writing – original draft, Visualization, Investigation, Formal analysis, Data curation. **Ning Chen:** Methodology, Formal analysis, Data curation, Conceptualization. **Dongxiao Liu:** Validation, Methodology. **Jionghan Wang:** Data curation. **Lin Chen:** Validation. **Xiaoguo Zhou:** Writing – review & editing, Supervision, Methodology, Investigation, Conceptualization. **Shilin Liu:** Supervision, Resources, Funding acquisition.

Declaration of competing interest

The authors declare that they have no known competing financial interests or personal relationships that could have appeared to influence the work reported in this paper.

Data availability

Data will be made available on request.

Acknowledgments

This work was financially supported by the National Natural Science Foundation of China (Nos. 22073088 and 22027801).

References

[1] F. Chiti, C.M. Dobson, Protein misfolding, functional amyloid, and human disease, Annu. Rev. Biochem 75 (2006) 333–366.
[2] J.D. Sipe, A.S. Cohen, History of the amyloid fibril, J. Struct. Biol. 130 (2000) 88–98.
[3] B.R. Bloem, M.S. Okun, C. Klein, Parkinson's disease, Lancet 397 (2021) 2284–2303.
[4] C. Duyckaerts, B. Delatour, M.-C. Potier, Classification and basic pathology of Alzheimer disease, Acta Neuropathol. 118 (2009) 5–36.
[5] C.M. Dobson, Protein folding and misfolding, Nature 426 (2003) 884–890.
[6] P. Cizas, R. Budvytyte, R. Morkuniene, R. Moldovan, M. Broccio, M. Lösche, G. Niaura, G. Valincius, V. Borutaite, Size-dependent neurotoxicity of β-amyloid oligomers, Arch. Biochem. Biophys. 496 (2010) 84–92.
[7] R. Kayed, C.A. Lasagna-Reeves, Molecular mechanisms of amyloid oligomers toxicity, J. Alzheimers Dis. 33 (2013) S67–S78.
[8] G. Merlini, V. Bellotti, A. Andreola, G. Palladini, L. Obici, S. Casarini, V. Perfetti, Protein aggregation, Clinical Chemistry and Laboratory Medicine (CCLM). 12 (2001) 1437–4331.
[9] C. Redfield, C.M. Dobson, Proton NMR studies of human lysozyme: spectral assignment and comparison with hen lysozyme, Biochemistry 29 (1990) 7201–7214.

[10] R. Swaminathan, V.K. Ravi, S. Kumar, M.V.S. Kumar, N. Chandra, Lysozyme: a model protein for amyloid research, Adv. Protein Chem. Struct. Biol. 84 (2011) 63–111.
[11] S.-Y. Ow, D.E. Dunstan, The effect of concentration, temperature and stirring on hen egg white lysozyme amyloid formation, Soft Matter 9 (2013) 9692–9701.
[12] D. Liu, N. Chen, T. Zhang, X. Zhou, S. Liu, The p H effects on thermal amyloid fibrillation kinetics of hen egg-white lysozyme using new normalization factor for Raman spectroscopy, J. Raman Spectrosc. (2024), https://doi.org/10.1002/jrs.6674.
[13] W. Fan, L. Xing, N. Chen, X. Zhou, Y. Yu, S. Liu, Promotion effect of succinimide on amyloid fibrillation of hen egg-white lysozyme, J. Phys. Chem. B 123 (2019) 8057–8064.
[14] W. Fan, X.-D. Chen, L.-M. Liu, N. Chen, X.-G. Zhou, Z.-H. Zhang, S.-L. Liu, Concentration-dependent influence of silver nanoparticles on amyloid fibrillation kinetics of hen egg-white lysozyme, Chin. J. Chem. Phys. 34 (2021) 393–405.
[15] W. Wang, S. Nema, D. Teagarden, Protein aggregation—Pathways and influencing factors, Int. J. Pharm. 390 (2010) 89–99.
[16] W.-T. Chen, Y.-H. Liao, H.-M. Yu, I.H. Cheng, Y.-R. Chen, Distinct effects of Zn2+, Cu2+, Fe3+, and Al3+ on amyloid-β stability, oligomerization, and aggregation: amyloid-β destabilization promotes annular protofibril formation, J. Biol. Chem. 286 (2011) 9646–9656.
[17] P. Zatta, R. Lucchini, S.J. van Rensburg, A. Taylor, The role of metals in neurodegenerative processes: aluminum, manganese, and zinc, Brain Res. Bull. 62 (2003) 15–28.
[18] J. Riordan, The role of metals in enzyme activity, Ann. Clin. Lab. Sci. 7 (1977) 119–129.
[19] N. Nelson, Metal ion transporters and homeostasis, EMBO J. 18 (1999) 4361–4371.
[20] S. Ghosh, N.K. Pandey, S. Bhattacharya, A. Roy, S. Dasgupta, Fibrillation of hen egg white lysozyme triggers reduction of copper (II), Int. J. Biol. Macromol. 51 (2012) 1–6.
[21] R. Chatterjee, V. Kolli, N. Sarkar, Trehalose and magnesium chloride exert a common anti-amyloidogenic effect towards hen egg white lysozyme, Protein J. 36 (2017) 138–146.
[22] X. Li, X. Chen, N. Chen, L. Liu, X. Zhou, S. Liu, Concentration-dependent effect of Nickel ions on amyloid fibril formation kinetics of hen egg white lysozyme: A Raman spectroscopy study, Chin. J. Chem. Phys. 36 (2023) 517–525.
[23] L. Liu, X. Li, N. Chen, X. Chen, L. Xing, X. Zhou, S. Liu, Influence of cadmium ion on denaturation kinetics of hen egg white-lysozyme under thermal and acidic conditions, Spectrochim. Acta A Mol. Biomol. Spectrosc. 296 (2023) 122650.
[24] X. Chen, L. Xing, X. Li, N. Chen, L. Liu, J. Wang, X. Zhou, S. Liu, Manganese Ion-Induced Amyloid Fibrillation Kinetics of Hen Egg White-Lysozyme in Thermal and Acidic Conditions, ACS Omega 8 (2023) 16439–16449.
[25] L. Xing, N. Chen, W. Fan, M. Li, X. Zhou, S. Liu, Double-edged effects of aluminium ions on amyloid fibrillation of hen egg-white lysozyme, Int. J. Biol. Macromol. 132 (2019) 929–938.
[26] J. Danielsson, R. Pierattelli, L. Banci, A. Gräslund, High-resolution NMR studies of the zinc-binding site of the Alzheimer's amyloid β-peptide, FEBS J. 274 (2007) 46–59.
[27] D.S. Gregory, A.C. Martin, J.C. Cheetham, A.R. Rees, The prediction and characterization of metal binding sites in proteins, Protein Eng. Des. Sel. 6 (1993) 29–35.
[28] B. Wang, T. Fang, H. Chen, Zinc and central nervous system disorders, Nutrients 15 (2023) 2140.
[29] B. Szewczyk, Zinc homeostasis and neurodegenerative disorders, Front. Aging Neurosci. 5 (2013) 33.
[30] F.C. Potocnik, S.J. van Rensburg, C. Park, J.J. Taljaard, R.A. Emsley, Zinc and platelet membrane microviscosity in Alzheimer's disease: the in vivo effect of zinc on platelet membranes and cognition, S. Afr. Med. J. 87 (1997) 1116–1119.
[31] Miller, Y., B. Ma and R. Nussinov (2010) Zinc ions promote Alzheimer Aβ aggregation via population shift of polymorphic states. *Proceedings of the National Academy of Sciences* **107,** 9490-9495.
[32] B. Ma, F. Zhang, X. Wang, X. Zhu, Investigating the inhibitory effects of zinc ions on amyloid fibril formation of hen egg-white lysozyme, Int. J. Biol. Macromol. 98 (2017) 717–722.
[33] D. Kurouski, T. Deckert-Gaudig, V. Deckert, I.K. Lednev, Surface characterization of insulin protofilaments and fibril polymorphs using tip-enhanced Raman spectroscopy (TERS), Biophys. J . 106 (2014) 263–271.
[34] V. Shashilov, M. Xu, V.V. Ermolenkov, L. Fredriksen, I.K. Lednev, Probing a fibrillation nucleus directly by deep ultraviolet Raman spectroscopy, J. Am. Chem. Soc. 129 (2007) 6972–6973.
[35] V. Sereda, I.K. Lednev, Polarized Raman spectroscopy of aligned insulin fibrils, J. Raman Spectrosc. 45 (2014) 665–671.
[36] N. Chen, Y. Ren, L. Xing, Z. Liu, L. Chen, S. Liu, X. Zhou, In situ Raman spectral observation of succinimide intermediates in amyloid fibrillation kinetics, Spectrochim. Acta A Mol. Biomol. Spectrosc. 309 (2024) 123867.
[37] N. Zaidi, M.R. Ajmal, S.A. Zaidi, R.H. Khan, Mechanistic in vitro dissection of the inhibition of amyloid fibrillation by n-acetylneuraminic acid: plausible implication in therapeutics for neurodegenerative disorders, ACS Chem. Nerosci. 13 (2021) 69–80.
[38] N. Zaidi, S. Nusrat, F.K. Zaidi, R.H. Khan, pH-dependent differential interacting mechanisms of sodium dodecyl sulfate with bovine serum fetuin: a biophysical insight, J. Phys. Chem. B 118 (2014) 13025–13036.
[39] D. Kurouski, R.P. Van Duyne, I.K. Lednev, Exploring the structure and formation mechanism of amyloid fibrils by Raman spectroscopy: a review, Analyst 140 (2015) 4967–4980.
[40] N. Kuhar, S. Sil, S. Umapathy, Potential of Raman spectroscopic techniques to study proteins, Spectrochim. Acta A Mol. Biomol. Spectrosc. 258 (2021) 119712.
[41] A.K. Dhillon, A. Sharma, V. Yadav, R. Singh, T. Ahuja, S. Barman, S. Siddhanta, Raman spectroscopy and its plasmon-enhanced counterparts: A toolbox to probe protein dynamics and aggregation, Wiley Interdiscip. Rev. Nanomed. Nanobiotechnol. 16 (2024) e1917.
[42] K. Shivani, A.A. Padhy, S. Sahoo, V. Kumari, P. Mishra, Spectroscopic methods to detect and analyze protein oligomerization, aggregation, and fibrillation, in: Advanced Spectroscopic Methods to Study Biomolecular Structure and Dynamics, Elsevier, 2023, pp. 415–458.
[43] T.G. Spiro, B.P. Gaber, Laser Raman scattering as a probe of protein structure, Annu. Rev. Biochem 46 (1977) 553–570.
[44] A. Barth, C. Zscherp, What vibrations tell about proteins, Q. Rev. Biophys. 35 (2002) 369–430.
[45] H. Takeuchi, Raman structural markers of tryptophan and histidine side chains in proteins. *Biopolymers: Original Research on*, Biomolecules 72 (2003) 305–317.
[46] T. Miura, H. Takeuchi, I. Harada, Raman spectroscopic characterization of tryptophan side chains in lysozyme bound to inhibitors: role of the hydrophobic box in the enzymic function, Biochemistry 30 (1991) 6074–6080.
[47] T. Miura, H. Takeuchi, I. Harada, Tryptophan Raman bands sensitive to hydrogen bonding and side-chain conformation, J. Raman Spectrosc. 20 (1989) 667–671.
[48] S. Dolui, A. Roy, U. Pal, A. Saha, N.C. Maiti, Structural insight of amyloidogenic intermediates of human insulin, ACS Omega 3 (2018) 2452–2462.
[49] L. Xing, K. Lin, X. Zhou, S. Liu, Y. Luo, Multistate mechanism of lysozyme denaturation through synchronous analysis of Raman spectra, J. Phys. Chem. B 120 (2016) 10660–10667.
[50] L. Xing, W. Fan, N. Chen, M. Li, X. Zhou, S. Liu, Amyloid formation kinetics of hen egg white lysozyme under heat and acidic conditions revealed by Raman spectroscopy, J. Raman Spectrosc. 50 (2019) 629–640.
[51] F.S. Parker, Applications of infrared, Raman, and resonance Raman spectroscopy in biochemistry, Springer Science & Business Media 128 (1983) 0005–9021.
[52] V. Receveur-Bréchot, J.M. Bourhis, V.N. Uversky, B. Canard, S. Longhi, Assessing protein disorder and induced folding. *Proteins: Structure*, Function, and Bioinformatics 62 (2006) 24–45.
[53] I.A. Kaltashov, S.J. Eyles, Mass spectrometry in biophysics: conformation and dynamics of biomolecules, John Wiley & Sons, 2005.
[54] S. Noguchi, K. Miyawaki, Y. Satow, Succinimide and isoaspartate residues in the crystal structures of hen egg-white lysozyme complexed with tri-N-acetylchitotriose, J. Mol. Biol. 278 (1998) 231–238.
[55] Y. Desfougères, J. Jardin, V. Lechevalier, S. Pezennec, F. Nau, Succinimidyl residue formation in hen egg-white lysozyme favors the formation of intermolecular covalent bonds without affecting its tertiary structure, Biomacromolecules 12 (2011) 156–166.
[56] T. Geiger, S. Clarke, Deamidation, isomerization, and racemization at asparaginyl and aspartyl residues in peptides. Succinimide-linked reactions that contribute to protein degradation, J. Biol. Chem. 262 (1987) 785–794.
[57] M. Xie, D. Vander Velde, M. Morton, R.T. Borchardt, R.L. Schowen, pH-induced change in the rate-determining step for the hydrolysis of the Asp/Asn-derived cyclic-imide intermediate in protein degradation, J. Am. Chem. Soc. 118 (1996) 8955–8956.
[58] S. Capasso, L. Mazzarella, F. Sica, A. Zagari, S. Salvadori, Spontaneous cyclization of the aspartic acid side chain to the succinimide derivative, J. Chem. Soc. Chem. Commun. (1992) 919–921.
[59] A. Rygula, K. Majzner, K.M. Marzec, A. Kaczor, M. Pilarczyk, M. Baranska, Raman spectroscopy of proteins: a review, J. Raman Spectrosc. 44 (2013) 1061–1076.
[60] Barth, A. (2007) Infrared spectroscopy of proteins. *Biochimica et Biophysica Acta (BBA)-Bioenergetics* **1767,** 1073-1101.
[61] S. Mangialardo, F. Piccirilli, A. Perucchi, P. Dore, P. Postorino, Raman analysis of insulin denaturation induced by high-pressure and thermal treatments, J. Raman Spectrosc. 43 (2012) 692–700.
[62] B. Hernández, F. Pflüger, S.G. Kruglik, M. Ghomi, Characteristic Raman lines of phenylalanine analyzed by a multiconformational approach, J. Raman Spectrosc. 44 (2013) 827–833.
[63] W.B. Fischer, H.H. Eysel, Polarized Raman spectra and intensities of aromatic amino acids phenylalanine, tyrosine and tryptophan, Spectrochim. Acta A: Mol. Spectrosc. 48 (1992) 725–732.
[64] C. Blake, D. Koenig, G. Mair, A. North, D. Phillips, V. Sarma, Structure of hen egg-white lysozyme: a three-dimensional Fourier synthesis at 2 Å resolution, Nature 206 (1965) 757–761.
[65] I. Harada, T. Miura, H. Takeuchi, Origin of the doublet at 1360 and 1340 cm− 1 in the Raman spectra of tryptophan and related compounds, Spectrochim. Acta A: Mol. Spectrosc. 42 (1986) 307–312.